Molecular Vision 2004; 10:577-87 <http://www.molvis.org/molvis/v10/a70>
Received 4 March 2004 | Accepted 20 August 2004 | Published 23 August 2004

The *ldis1* lens mutation in RIIIS/J mice maps to chromosome 8 near *cadherin 1*

Monica M. Jablonski,[1,2] Lu Lu,[2] XiaoFei Wang,[1,2] Elissa J. Chesler,[2] Emily Carps,[2] Shuhua Qi,[2] Jing Gu,[2] Robert W. Williams[2]

[1]Department of Ophthalmology, [2]Center of Genomics and Bioinformatics, University of Tennessee Health Science Center, Memphis, TN

Purpose: We have discovered a spontaneous and severe mutation that leads to partial or complete disruption of the lens and cataract in the RIIIS/J inbred strain of mice. The purpose of this study was to determine the mode of inheritance, specificity, and range of phenotypes using histological, ophthalmic, quantitative electron microscopic, and microarray-based methods. We also have fine-mapped the mutation, *ldis1* (lens disrupter 1), and have evaluated positional candidate genes.

Methods: Eyes from mutant RIIIS/J animals and from an F2 intercross between RIIIS/J and DBA/2J were examined and scored to map the *ldis1* mutation. Axons in the optic nerve were counted. Messenger RNA from mutant eyes was hybridized to Affymetrix short oligomer microarrays and compared to five control strains. Expression differences were used to evaluate molecular sequellae of the mutation.

Results: Mice that are homozygous for *ldis1* have small eyes. Lenses are without exception opaque, deformed, dislocated, fragmented, and small. In contrast, retinal architecture and ganglion cell numbers are within normal range. We have not detected any other *ldis1*-associated ocular or systemic abnormalities. *ldis1* is recessive and maps to chromosome 8 at about 106.5 Mb between *D8Mit242* and *D8Mit199* with a peak LOD score near *cadherin 1*. The homologous human chromosomal interval is 16q22.1. The expression of several downstream crystallin transcripts are severely affected in the mutant, as are the expression levels of multiple members of the transforming growth factor superfamily and the glutathione S-transferases.

Conclusions: We have discovered and mapped a recessive mutation to mouse chromosome 8 between 105 and 109 Mb. Homozygous mutant mice have a selective and severe effect on lens integrity. On the basis of the phenotype and the locus position, several candidate genes have been identified.

Congenital cataracts are a significant cause of visual impairment and blindness with a prevalence rate of approximately 0.01-0.06%. They may develop during embryogenesis, at birth, or shortly after birth and usually manifest as a disruption of lens architecture (reviewed in [1]). Isolated cataracts are usually inherited in a Mendelian fashion with dominant transmission being the most frequent inheritance pattern. As of 2003, 27 genetic loci for isolated or primary cataract have been mapped in humans, eight of which are associated with other developmental syndromic abnormalities (reviewed in [1]). In addition, cataracts and associated anterior ocular malformations are frequently associated with mild or severe microphthalmia due to the organizing effect of the lens on other intraocular structures [2].

While there has been tremendous progress in determining the genetic causes of human cataract (reviewed in [1]), the small size of available families can limit the ability to isolate the causative gene. Moreover, the molecular mechanisms leading to the cataractous phenotype often remain elusive. In these instances, an appropriate animal model is useful to determine the mechanisms involved in cataract formation and the identification of the causative gene. Some laboratories have implemented a mutagenesis approach including the use of X-rays and ethylnitrourea to induce mutant models of cataract. Using these strategies, approximately 200 independent lines of cataract mutants have been generated by mutagenesis and are maintained at Neuherberg [3].

In this study, we have identified and characterized a spontaneously occurring non-syndromic mutant mouse, the RIIIS/J inbred strain that manifests with a severe lens abnormality associated with a consistent reduction in total eye size. We have mapped the causative gene locus to a 4 Mb interval on chromosome 8 and named this gene *ldis1* (lens disruptor 1). We have also identified several candidate genes based upon locus position and biological evidence presented in the literature. Changes in the gene expression profiles of eyes from homozygous RIIIS/J mutants have also been compared to those from wildtype mice, a method that has allowed us to identify downstream effects of the *ldis1* mutation.

METHODS

Animals: The use of animals in this study were used in compliance with the Guiding Principles in the Care and Use of Animals (DHEW Publication NIH 80-23), the Declaration of Helsinki, and was approved by the Animal Care and Use re-

Correspondence to: Monica M. Jablonski, Ph.D., Department of Ophthalmology, 956 Court Avenue, Suite D228, Memphis, TN, 38163; Phone: (901) 448-7572; FAX: (901) 448-5028; email: mjablonski@utmem.edu

view board of the University of Tennessee Health Science Center. Three complementary groups of mice were used to characterize the phenotype and map the responsible gene. The first group consisted of 77 fully inbred RIIIS/J animals. The second group was comprised of 24 F1 intercross progeny between RIIIS/J and DBA/2J parental strains. The third group of mice consisted of 231 F2 intercross progeny. Parental stocks were obtained from the Jackson Laboratory (Bar Harbor, ME). Wildtype mice (C57BL/6J, C57BL/6ByJ, DBA/2J, and CXB RI strains) were used as controls to assess transcripts that may be affected directly or indirectly by the *ldis1* mutation. Mice were maintained at 20-24 °C on a 14/10 h light/dark cycle in a pathogen-free colony at the University of Tennessee Health Science Center. Animals were fed a 5% fat Agway Prolab 3000 rat and mouse chow and given tap water in glass bottles.

Ophthalmic examination: Mice at nine weeks of age (RIIIS/J, n=3; DBA/2J, n=3) were lightly anesthetized with an intraperitoneal injection of Avertin (1.25% 2,2,2-tribromoethanol and 0.8% tert-pentyl alcohol in water, 0.3 ml). Eyes were examined with a slit lamp biomicroscope (Carl Zeiss, Germany). Images of the cornea and lens were recorded with a Canon GL1 digital video camera (Canon U.S.A., Inc., Lake Success, NY) via a video adapter (Transamerican Technology International, Sam Ramon, CA). After examination of the anterior segment, the eyes were dilated with 1% Cyclomydril ophthalmic drops (Alcon Pharmaceuticals, Fort Worth, TX). The fundus was evaluated by indirect ophthalmoscopy and photographs were taken with a Kowa Genesis small animal fundus camera (Torrance, CA) along with the aid of a 90 diopter condensing lens (Volk, Mentor, OH) as described previously [4,5].

Eye and lens weight, and ocular morphology: Six groups of mice (age range 49-99 days; n=393; please see Table 1 for distribution of mice among the six groups) were killed by cervical dislocation and eyes were immediately removed. Extraocular tissues were trimmed and eyes were weighed individually on a microbalance, followed by fixation with 4% paraformaldehyde in 0.06 M phosphate buffer. After 24 h in fixative, lenses (n=213) were removed from the majority of the eyes with the aid of a dissection microscope, and were weighed separately. In addition, the morphology of the lenses was graded and lenses were categorized as normal or abnormal depending upon the shape and integrity of each lens. Eye and lens weight data were statistically analyzed using DataDesk 6.1.

Eyes that were used for ocular histology (age range 98-235 days; RIIIS/J, n=10; DBA/2J, n=5; F2 intercross progeny, n=10) were fixed in 4% paraformaldehyde followed by paraffin embedding and sectioning using standard protocols. The orientation of the eyes during embedding was controlled so that the anterior-posterior axis of the eye was parallel to the cutting surface of the block. Sections were cut at 12 μm through the entire eye and those in which the optic nerve peaked in thickness were evaluated morphologically. Representative tissue sections were stained with hemotoxylin and eosin. Sections were viewed on an Eclipse E800 microscope (Nikon Inc., Tokyo, Japan) equipped with a color camera (Photometrics, Tucson, AZ), and the images were collected with MetaMorph software (Universal Imaging Corporation, West Chester, PA).

Mice (age range 44-99 days; RIIIS/J, n=5; F1 intercross progeny, n=5) used for electron microscopic analysis of the optic nerves were anesthetized deeply with Avertin and perfused transcardially with mixed aldehydes. The processing and analytic procedures used to count axons of retinal ganglion cells following the procedures as detailed in Williams et al. [6].

Genotyping: The genotypes of individual mice were determined using a method described previously [7]. In brief, genomic DNA was obtained from the spleens of a set of 231 F2 mice. Microsatellite primer pairs were purchased from Research Genetics (Huntsville, AL; which has since been acquired by Invitrogen Life Technologies, Carlsbad, CA). PCR reactions were carried out in 96-well microtiter plates. A high-stringency touchdown protocol was used in which the annealing temperature was lowered progressively from 60 °C to 50 °C in 2 °C steps over the first 6 cycles [8]. After 30 cycles, products from the PCR reactions were run on 2.5% Metaphor agarose gels (FMC Bioproducts, Rockland, ME), stained with ethidium bromide, and photographed. A set of 67 MIT microsatellite loci [9] distributed across all autosomes and the X chromosome were typed, initially using only a subset of 45 adult animals with unusually small eyes (<15 mg; age range 44-99 days). After detection of linkage on chromosome 8, all 231 F2 progeny were genotyped for a set of 9 MIT markers between on chromosome 8. Genotypes were entered into Microsoft Excel and transferred to the Map Manager QTX programs (version b17) for mapping and permutation analysis [10]. QTX implements both simple and composite interval mapping methods, as has been previously described [11]. Genome-wide significance levels for assessing the confidence of the linkage statistics was estimated by comparing the peak likelihood ratio statistic (LRS) of correctly ordered data sets with LRS values computed for 10,000 permutations [12]. LRS scores were converted to logarithm of odds ratios (LOD scores) by dividing the LRS value by 4.6. All MIT microsatellite and gene positions are based on the Mouse Genome Sequencing Consortium build of February, 2003 (Mouse Genome Browser).

RNA extraction and transcript mapping: To determine the downstream effects of the *ldis1* mutation, mRNA levels of

Table 1. Eye weights from unfixed left eyes, grouped by genotype

Strain	RIIIS/J	DBA/2J	F1 intercross progeny	F2 progeny D/D at Ids1 locus*	F2 progeny D/R at Ids1 locus*	F2 progeny R/R at Ids1 locus*
Mean	16.5	21.2	23.8	18.9	19.7	14.0
SD	4.0	4.0	3.3	2.7	2.8	3.9
SEM	0.5	0.5	0.7	0.4	0.3	0.5
n	77	61	24	47	113	53

Presented in this table are the weights from the unfixed left eyes from F2 mice. The data are segregated by mouse genotype at the *ldis1* locus. The asterisk indicates genotype at markers *D8Mit242* and *D8Mit199*. The "R" indicatges the RIIIS/J genotype and "D" indicates the DBA/2J genotype.

whole eyes (age range 44-99 days) from RIIIS/J mice were compared with those of several wildtype inbred strains. The use of whole eyes, as opposed to isolated lenses, was selected in these studies for several reasons. First, the purpose of this investigation was to assess the global ocular effects of the *ldis1* mutation. And second, because we do not know that the primary genetic defect is in the lens, using isolated lenses could lead to false negative results. Pools of four eyes per Affymetrix U74Av2 chip were processed to extract total RNA using TRIzol reagent (GibcoBRL, Gathersburg, MD) and stored in RNALater (Ambion, Inc. Austin, TX). The number of arrays that were analyzed per strain is as follows: RIIIS/J, n=3; C57BL/6J, n=4; C57BL/6ByJ, n=1; DBA/2J, n=4; CXB RI strains, n=3. RNA quality and purity was assessed using an Agilent Bioanalyzer 2100 system (Agilent Technologies, Palo Alto, CA). All samples were of sufficient quality to generate cDNAs and cRNAs. RNA was used to synthesize first and second strand cDNA, which was subsequently utilized to produce biotinylated cRNA following the protocol recommended by Affymetrix (Santa Clara, CA). Labeled cRNA probes were prepared and hybridized to the Affymetrix U74Av2 arrays according to the protocols provided by the manufacturer. All procedures other than hybridizations were performed at The University of Tennessee Health Science Center, while Genome Explorations Inc. (Memphis, TN) performed the hybridizations.

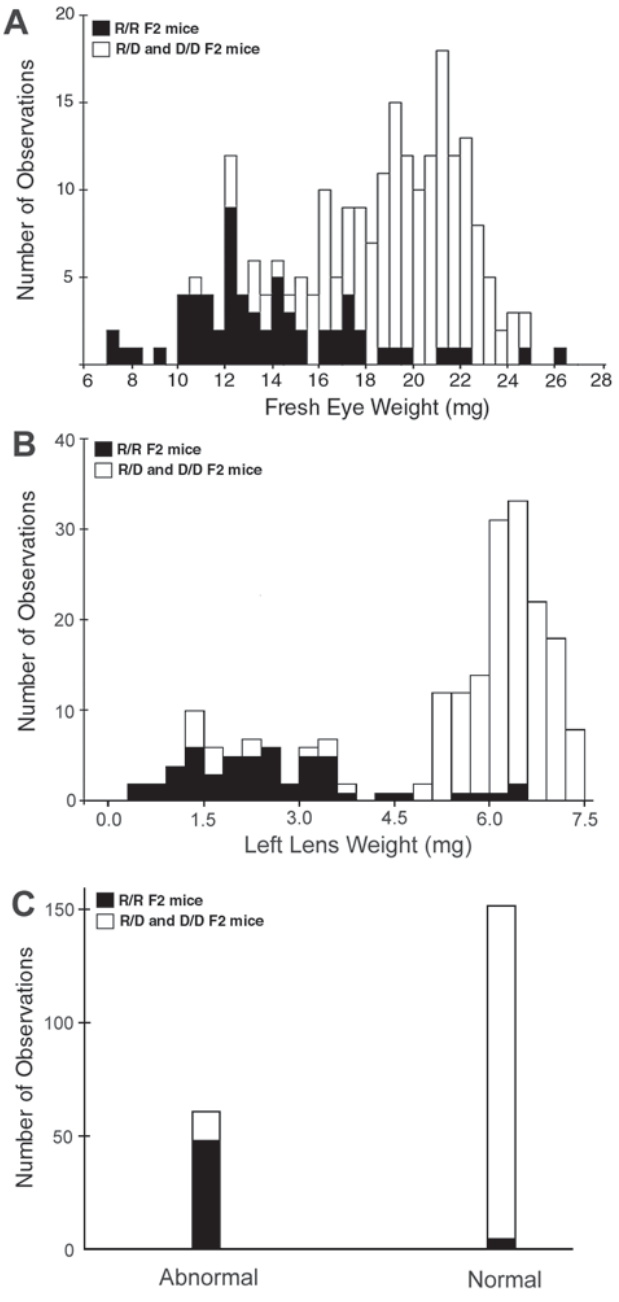

Figure 1. Graphical illustrations of eye and lens weights along with lens morphology, grouped by genotype. Stacked histograms indicating the number of observations documented for fresh eye weights (**A**), lens weights of left eyes (**B**), and lens morphology (**C**) in all F2 mice. Black bars indicate the values from F2 mice that were homozygous for the RIIIS/J allele (R/R) at both markers, *D8Mit242* and *D8Mit100*. White bars indicate heterozygous (R/D) and/or wildtype (D/D) F2 mice.

Array data generation and preprocessing: Scanner output image files were processed using MAS 5.0 (Affymetrix, Inc., Santa Clara, CA). Data files for the U74Av2 microarray consists of about 12,422 rows of expression values and ancillary data with additional rows for exogenous control mRNA used for quality control. Each row summarizes the expression level of a single transcript (probe set) generated using data from a total of 32 probes grouped into 16 perfect match-mismatch pairs (see Affymetrix Statistical Algorithms Description white paper for descriptions of methods used in the evaluation of Affymetrix microarray data). Each probe set is designed to target a single gene transcript, usually with an intentional bias toward the 3' UTR end of the transcript. Approximately 25% of the all probe sets are actually duplicates and thus many probe sets target the same gene. Hence the arrays actually target transcripts of approximately 9,000 genes. The MAS 5.0 expression values assigned to each probe set range from 0 to approximately 50,000.

To normalize, combine, and compare data from different arrays, we computed the logarithm (base 2) of the original MAS 5.0 hybridization signal for each array experiment. To avoid negative values after the log transformation, we added a constant of 1 to all values prior to the log transform. Log base 2 was chosen for ease of interpretation (each unit represents roughly a two fold difference in expression level). Finally, we rescaled data for each array to a mean value of 8 and stabilized the variance to a value of 4. To improve data reliability, we ran three replicate arrays using RNA pools isolated from three separate groups of RIIIS/J mice. These data were compared to arrays from wildtype mice using a relatively conservative t-test that assumes unequal variance between groups. Given the large numbers of comparisons in microarray studies, typical family-wise adjustments required to control for false positives are unduly stringent. We therefore calculated the false discovery rate, a method that helps to estimate how many false positives are expected in set of transcripts for which the null hypothesis is rejected at a particular significance

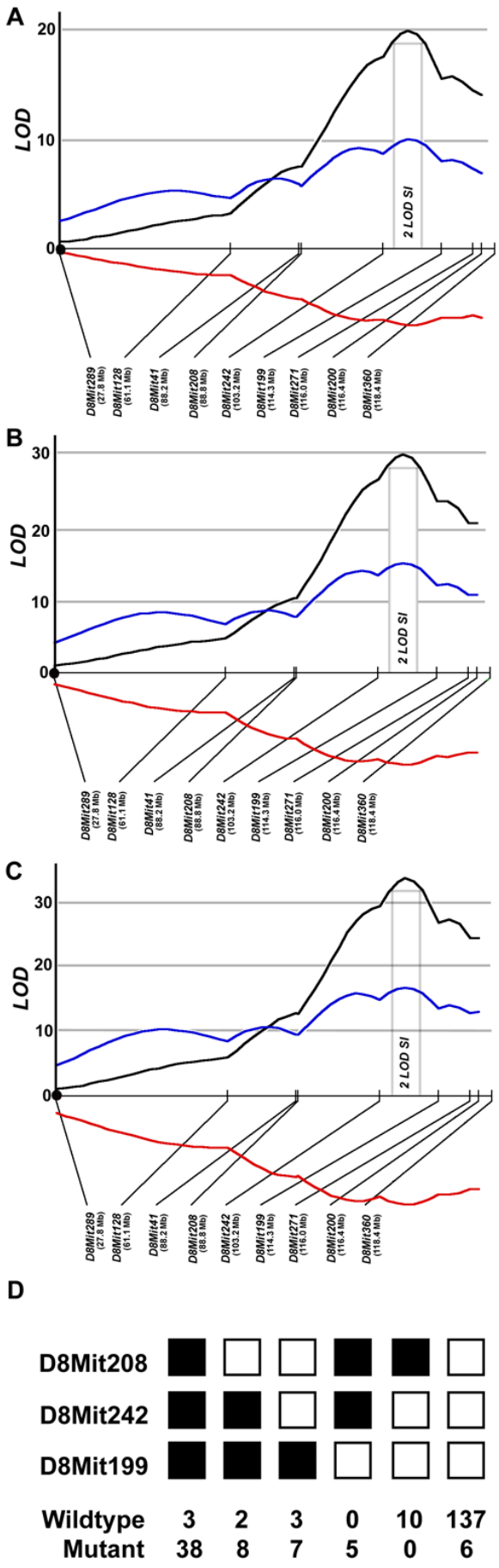

threshold. Computation of q values provides an assessment of the number of false results one would obtain if declaring a particular transcript significant (and thus all others with smaller p values), along with the total number of truly significant findings in the entire set [13].As always, expression differences detected in this study should be considered provisional until reproduced using independent methods.

RESULTS

Eye and lens weights: The RIIIS/J mutation was originally detected because eye weights of this strain are unusually low in comparison to those of over 50 other strains of mice we have characterized [14,15]. The average eye size of the RIIIS/J mutant strain is significantly smaller than that of the DBA/2J strain that we used for the test cross to map the mutation (16.5 mg versus 21.2 mg; Table 1, $p<0.05$). Nine of 77 RIIIS/J mutants had eye weights less than 15 mg. R3D2 F1 mice which are obligate heterozygotes for the mutation have eye weights that are slightly heavier than those of animals that are wildtype (23.8 mg versus 21.2 mg, Table 1), suggesting a slight overdominant effect of the mutation. Lenses of the heterozygotes are not morphologically distinguishable from normal. The population of F2 mice have eye weights with a bimodal distribution in which roughly 25% of animals belong to a low mode (65 animals with eye weights <15 mg) and roughly 75% belonging to the high mode (166 animals with eye weights >15 mg, Figure 1A).

ldis1 *gene locus: Effect upon eye and lens weight and lens morphology:* The RIIIS/J mutation maps to Chr 8 (Figure 2). The interval map was determined using three phenotypes, namely eye weight (Figure 2A), lens weight (Figure 2B), and lens morphology (Figure 2C), all of which are associated with the RIIIS/J phenotype. In all instances, the measurement in question of the F2 progeny is associated with an extremely high LOD score of 20, 30, and 37, respectively, centered around the *Cdh1* gene. The mode of inheritance at this locus is consistent with a recessive mode of inheritance of the mutant allele and its effect on eye and lens. This locus, termed *ldis1* is flanked proximally by marker *D8Mit242* (101.6 Mb or 48 cM)

Figure 2. Interval map of *ldis1* on chromosome 8. The x-axis represents all of chromosome 8 from the centromere (black dot) near marker *D8Mit289* to the telomere near *D8Mit360*. Black line graphs the LOD score of linkage of data based upon eye weight (**A**), lens weight (**B**), and lens morphology (**C**). The blue line graphs represent the coefficent of the wildtype allele dominance whereas the red lines represent the coefficient of the additive effect. Values in parentheses next to markers are megabase positions from the October 2003 mouse genome assembly (UCSC version mm4), which is based on NCBI Build 32. The 2-LOD support interval (SI) of *ldis1* is bracketed between *D8Mit242* and *D8Mit199* in each figure. **D**: Haplotype analysis of the *ldis1* region on distal chromosome 8 between *D8Mit242* and *D8Mit199*. Black squares indicate the R/R genotype, while white squares indicate heterozygous (R/D) and/or wildtype (D/D) mice. The number of progeny from the R/R and R/D or D/D genotypes are indicated under each haplotype. The genotype of some of the mice with the R/D heterozygous genotype suggest that the *ldis1* locus is not entirely recessive.

and distally by marker *D8Mit199* (112.5 Mb or 56 cM; see Figure 2). The 2-LOD support interval, a very conservative estimate of the 95% confidential interval likely to include the mutated gene, is approximately 4 Mb and extends from *Cbfb* to *Atbf1* (Figure 3).

With knowledge of the location of the *ldis1* locus, the distribution of eye weights of the 231 F2 mice can be split into two groups; those that are homozygous for the mutant RIIIS/J interval at *ldis1* and all other F2 mice. The average eye weight of the *ldis1* mutants that are homozygous mutants (R/R genotype at both flanking markers) is reduced significantly compared to the other F2 mice (Table 1). Note however that the mutants do not form a completely isolated mode in Figure 1. A small number of mutants have normal or even abnormally large eyes and a small proportion of non-mutants have small eyes. This is due to the segregation of many other normal gene variants that affect eye size in mice [14,15].

In a manner paralleling eye weights, the lens weights of the F2 mutants are also reduced compared to mice that are wildtype or homozygous at the *ldis1* locus ($p<0.001$, Table 2 and Figure 1B). When evaluated for morphologic appearance, the great majority of the lenses of the homozygous F2 mutants are abnormal, whereas those of the homozygous and wildtype F2 mice are with very few expections perfectly normal (Figure 1C). Moreover, lenses with an abnormal morphology have a significantly reduced lens weight compared to those with a normal morphology ($p<0.0001$, Table 3). Together these data demonstrate that the weight of the lens is highly correlated with lens morphology.

Table 2. Lens weights from fixed left eyes, grouped by genotype

Strain	F2 progeny D/D at Ids1 locus*	F2 progeny D/R at Ids1 locus*	F2 progeny R/R at Ids1 locus*
Mean	5.8	6.0	2.5
SD	1.1	1.3	1.5
SEM	0.2	0.1	0.2
n	47	113	53

Presented in this table are the lens weights obtained from paraformaldehyde-fixed left eyes from F2 mice. The data are segregated by mouse genotype at the *ldis1* locus. The asterisk indicates genotype at markers *D8Mit242* and *D8Mit199*. The "R" indicatges the RIIIS/J genotype and "D" indicates the DBA/2J genotype.

Table 3. Lens weights from fixed left eyes, grouped by lens morphology

Strain	n	Mean	SD	SEM
Normal lens	152	6.3	0.6	0.0
Abnormal lens	61	2.2	1.0	0.1

Presented in this table are the lens weights obtained from paraformaldehyde-fixed left eyes from F2 mice. The data are segregated by morphology of the lens.

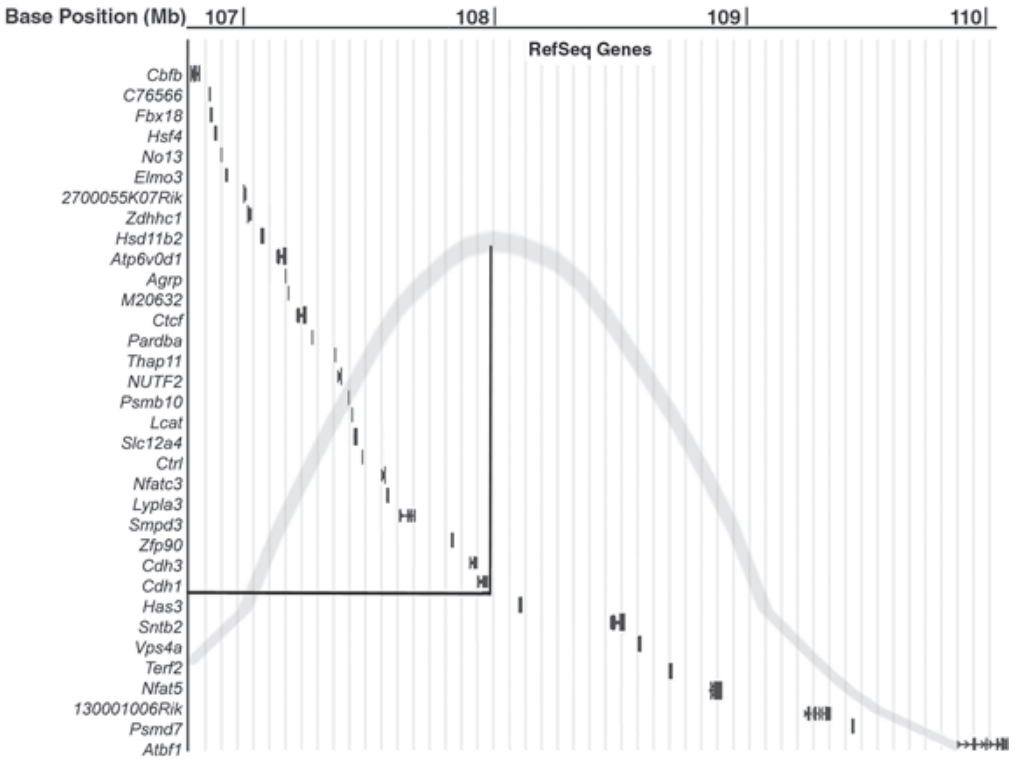

Figure 3. Genes contained in the 2-LOD support interval of *ldis1*. 2-LOD support interval of *ldis1* (light grey curve) superimposed on a Genome Browser view of chromosome 8 from 106.6 to 110.4 Mb (October, 2003 assembly, mm4). Thirty-four positional candidate genes (from *Cbfb* to *Atbf1*) are listed in positional order on chromosome 8. *Cdh1* is located near the peak of the 2-LOD significance interval.

Slit lamp biomicroscopy: Representative images obtained from the slit lamp biomicroscope are shown in Figure 4. At 9 weeks of age in the RIIIS/J mouse, the intraocular lenses are dislocated temporally, rather than being centered in the visual axis. Moreover, the lenses of all RIIIS/J mice are opaque (Figure 4A). The cataract presents with cortical and nuclear manifestations. The fundi of RIIIS/J mice cannot be seen with the indirect ophthalmoscope because of the lens opacity. In contrast, the lenses of DBA/2J mice are transparent and centered in the visual axis (Figure 4B).

Ocular histology and optic nerve axon quantification: Histological analysis reveals severe abnormalities in lens structure (Figure 5A,B). The lens of RIIIS/J mice fail to form a spherical shape and frequently the lens capsule has become disrupted thus allowing lens fibers to migrate behind the posterior lens capsule. In addition, the epithelial cells that normally terminate at the lens equator often circumscribe the entire lens in RIIIS/J mice. Nuclei of lens fiber cells are found throughout the lens of the RIIIS/J mutants, indicating that the degradation of cell nuclei is inhibited in these mice. The fibers of the entire lens are stained much more intensely with the hemotoxylin stain, similar to the staining intensity of the less mature fibers of the non-mutant mouse (compare to Figure 5C,D). This pattern of staining is consistent with denatured and precipitated protein in the lens. Other than the lens, all other ocular structures, including the retina, appear normal morphologically (Figure 5A). An identical ocular morphology is present in mutant F2 intercross progeny, the mutant status of which was determined by genotyping (data not shown).

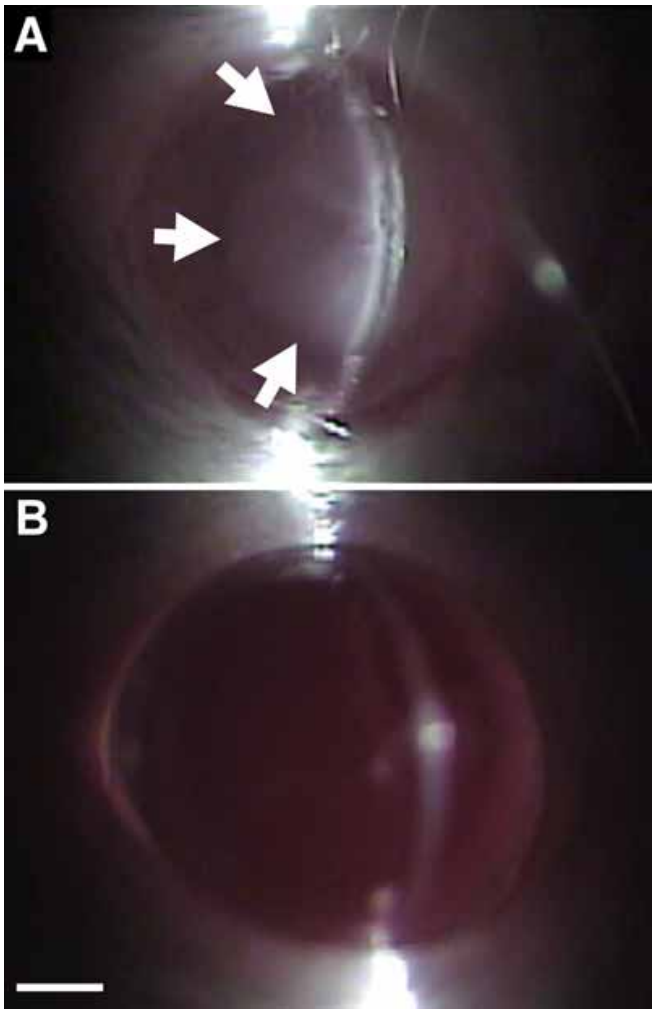

Figure 4. Comparative examination of the lens of RIIIS/J and wildtype mice. Images from the lens in nine-week-old parental strains of mice as seen with a slit lamp biomicroscope. By ophthalmic exam, the lens is opaque and translocated temporally in RIIIS/J mice (**A**, white arrows). This in contrast to the transparent and centered lens of the DBA/2J parental strain (**B**). The magnification bar is equal to 1 mm.

In F2 mice that are wildtype at both markers flanking *ldis1*, all ocular structures appeared normal on morphologic inspection. The lens is spherical and of normal size and shape (Figure 5C,D). All ocular structures in heterozygous F2 progeny are also morphologically identical to those of non-mutant F2 mice (data not shown).

Ganglion cell axon counts within the optic nerves of both RIIIS/J and F1 intercross progeny are within the range normally seen in inbred strains of mice (51,620±2,315 and 55,988±2,023, respectively). We have previously demonstrated that the ganglion cell axon counts of inbred laboratory strains ranges from approximately 50,000 to 66,000, depending upon the strain [6]. In addition, we did not observe any necrosis of the axon under any condition. Together our histological and optic nerve count data suggest that the retina of the RIIIS/J mice was not affected by the *ldis1* mutation.

RNA transcript mapping: q Values were calculated for all transcripts using the q value R code [13]. The q values indicate the number of false positive results in the set of genes that would be rejected if a particular gene and those with lower p values were considered significantly altered. This approach is more informative than the use of a cut-off, which arbitrarily rejects potentially interesting results despite biological evidence. It was estimated from our data that 28.3% of the results are truly significant for a total of 3,031 of the transcripts (Figure 6A). However, it is impossible to determine exactly which transcripts these are. As more genes are declared significant, the percentage of false positive results increases. At a false discovery rate of 20%, 1,150 genes would be considered positives and 230 of these results (20%) will be truly non-significant (Figure 6B).

A mutation such as *ldis1* has serious effects on the morphology of the lens and the size of the whole eye. Because of this, it was critical to include the entire eye in our quest to determine which RNA transcripts differ in the RIIIS/J mutant. In our analysis of the transcripts that were differentially regulated in RIIIS/J mice, we initially focused on the expression levels of all transcripts whose genes lie within the 2-LOD support interval shown in Figure 5. Of the genes in this region, the levels of only two transcripts were altered in RIIIS/J mice. The esterase 31 transcript (*Es31*) at 104.9 Mb is elevated in the RIIIS/J mouse (p=0.0221, q=0.1817, 2.5 fold increase) whereas the core binding protein beta (*Cbfb*) is decreased (p=0.0275, q=0.1935, 1.3 fold reduction in the RIIIS/J mouse).

The heat shock transcription factor 4 (*Hsf4*) is decreased by 2.2 fold in the RIIIS/J mouse, although this value does not achieve significance using a conventional t-test (p=0.1098, q=0.3372). No other transcript levels differ appreciably between the RIIIS/J mice and wildtype controls within the 2-LOD support interval. To look for alterations outside of the 2-LOD support interval, we also screened for abnormalities in transcript expression across the whole genome (Figure 7). Of course, not all gene transcripts are represented on the Affymetrix U74Av2 array, so there may be alterations in specific pathways that we are not able to detect. Nonetheless, as expected, many of the crystallins (*Crygd*, *Cryge*, *Crygf*, and *Crym*), are dramatically downregulated in eyes from RIIIS/J mutants (p=0.0104, q=0.1413; p=0.0119, q=0.1470; p=0.0206, q=0.1800 and; p=0.0002, q=0.0512, respectively). However, this is not unexpected given the overlapping sequences between the crystalline probes used in the U74Av2 microarrays.

The levels of several other transcripts were significantly altered in the RIIIS/J mutant, including multiple members of the transforming growth factor superfamily, i.e., transforming growth factor (TGF), fibroblast growth factor (FGF), the bone morphogenic proteins (BMP) and the activins. Specifically, levels of *Bmp7*, *Bmpr1b*, *Fgf1*, *Fgf12*, *Tgfa*, and *Tgfb1i4* are elevated in eyes from the RIIIS/J mutant (p=0.0245, q=0.1869; p=0.0011, q=0.0736; p=0.0151, q=0.3848; p=0.0009, q=0.0736; p=0.0075, q=0.1282, and p=0.0002, q=0.0512, respectively), while *Acvr1b*, *Fgf7*, and *Tgfb1* are decreased (p=0.0011, q=0.0736; p=0.0244, q=0.1869, and p=0.0262, q=0.1916, respectively). Moreover, another cluster of transcripts, the glutathione S-transferases (GST), are synergistically downregulated in the *ldis*1 mutant. For each of the four GST transcripts that are represented on the U74Av2 array, the expression level is lower in eyes from the RIIIS/J mutant compared to the wildtype controls (p values range from 0.018 to 0.000002, q ranges from 17% to 0.3%).

DISCUSSION

We have identified a novel mutant mouse that presents with a primary lens phenotype. Homozygous RIIIS/J mutant mice have unusually small eyes and cataractous lenses. The lens is dysmorphic with lenticular tissue present behind the posterior lens capsule, suggestive of a disruption of the capsule itself. All other ocular structures appeared morphologically normal. No systemic abnormalities were apparent, likely explaining why this mutation has gone undetected even though the RIIIS/J mouse is a common inbred strain. We compared this new

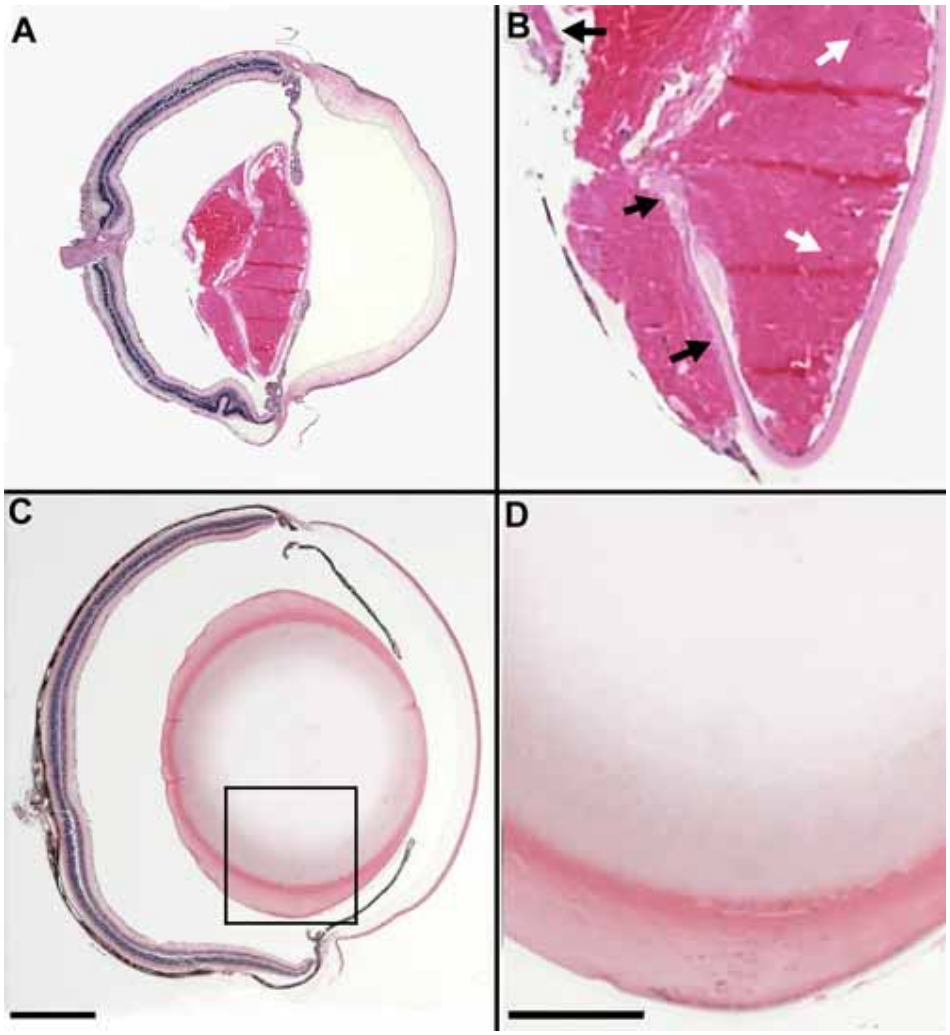

Figure 5. Comparative ocular histology of RIIIS/J and wildtype mice. Examples of the ocular histology of an RIIIS/J mouse (**A** and **B**) and a non-mutant F2 intercross progeny (**C** and **D**). Both the eye and lens of the RIIIS/J mouse are considerably smaller than that of the non-mutant mouse. In addition, histologic analysis reveals severe abnormalities in lens structure. In all RIIIS/J mice, the lens fails to form a spherical shape and lens tissue is present behind the lens capsule within vitreous chamber of the eye. Moreover, the epithelial cells circumscribe the lens (black arrows), rather than terminating at the lens equator (**A** and **B**). Nuclei fail to degrade in the lens fiber cells of the mutant mouse (white arrows). There are no apparent abnormalities in the eyes of non-mutant mice. Insets in **A** and **C** are magnified in **B** and **D**, respectively. The magnification bars are equal to 1 mm.

mutant model with previously reported murine cataracts and determined that the phenotype generated by a mutation in *ldis1* is unique.

By performing an entire genome linkage search, we narrowed the locus of the *ldis1* mutation to a 4 Mb interval bracketed by *Es31* and *Atbf1*. Within the 2-LOD significance interval are at least 34 candidate genes, 28 of which have known or proposed functions. Of those 28 genes, there are at least four plausible candidates that could be associated with the *ldis1* mutation. The first of these candidates is *Hsf4* that encodes for heat shock transcription factor 4. *HSF4* was recently identified as being the causative gene responsible for Marmer's cataract in a Danish family and a lamellar cataract in a Chinese family [16]. A second candidate is *Zfp90*, which encodes zinc finger protein 90. While this specific gene product has not been localized specifically to the eye, another zinc finger clone, *pMLZ-4*, has been isolated from the lens of the mouse eye [17], suggesting that members of this superfamily are present in and expressed by specific ocular cell types and may play a role in ocular genesis. *Cdh1*, which encodes for cadherin 1 or E-cadherin, is located at the peak of the 2-LOD significance interval of *ldis1*. The *Cdh1* gene product has been demonstrated to localize to several ocular structures including the lens epithelium. In this location, the other ocular cadherins (i.e., P- and N-cadherin) are not expressed [18] although the gene for P-cadherin or *Cdh3* is also positioned near the peak of our 2-LOD significance interval, thus suggesting that a mutation in the gene coding for E-cadherin would not be compensated for by the presence of another cadherin and a primary lens phenotype would likely occur. It is worth noting that three other cadherin genes (i.e., *cdh5*, *cdh11*, and *cdh16*) are localized just outside of our 2-LOD significance interval, thus they may also be candidate genes for *ldis1*. Both *cdh5* [19,20] and *cdh11* [21,22] have been localized to the eye, while there has been no documented expression of *cdh16* to any ocular structure. The final candidate gene that we consider highlighting is *Has3*. *Has3* encodes for hyaluronan synthase 3, which is an enzyme necessary to produce hyaluronan. This glycosaminoglycan is produced by lens epithelial cells and has been linked to posterior capsule opacification [23]. The last three candidates, *Zfp90*, *Cdh1*, and *Has3*, are clustered at the peak of the 2-LOD interval between 106.3 to 106.7 Mb.

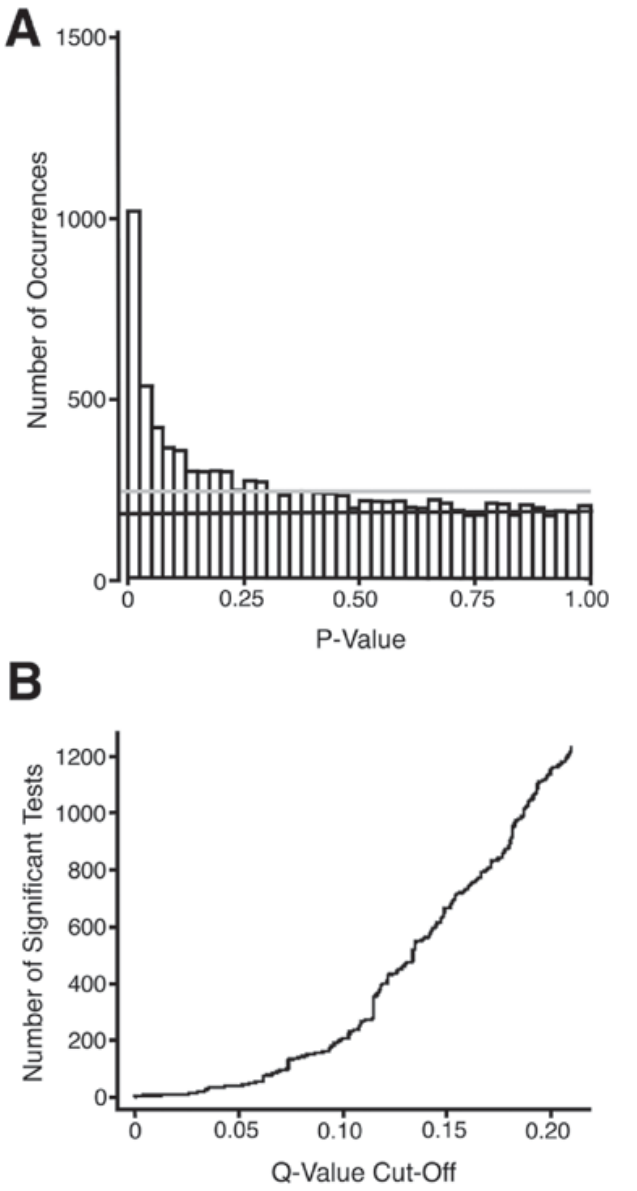

Figure 6. p Value distributions and q value cut-off values. **A** illustrates a frequency histogram of the p values obtained in the array analysis. The pale grey horizontal line indicates the distribution of p values under the assumption that all tests are truly non-significant. The darker horizontal line indicates the uniform distribution of p values expected in this data set, with 71.7% of the tests truly non-significant. The frequency of tests above this line is the frequency of truly significant results estimated in each p value bin of the histogram. **B** illustrates the number of rejected tests at a given q value. Note that for a q value of 0.2, 1150 genes are declared significant, and 20% or 230 of these rejected tests are false discoveries.

The *ldis1* critical region corresponds to human chromosome 16q22. Earlier studies have mapped cataract genes to chromosome 16q22.1 in human. Loci for a progressive posterior polar cataract and the Marner's cataract have been assigned to this interval on chromosome 16 [24,25]. Recently, the gene responsible for the development of these cataract phenotypes has been identified as *HSF4*, thus demonstrating that the same gene product is capable of generating distinct phenotypes depending upon which domain of the protein product is affected by the mutation. Even though the cataract phenotype we document in the RIIIS/J mutant mouse is distinct from the presentation found in humans with mutations in *HSF4*, it is plausible that this same gene is responsible for the phenotype seen in RIIIS/J mice, given the presence of *Hsf4* within the 2-LOD support interval of *ldis1* and its biological role in the lens. Exactly which gene is mutated in the RIIIS/J mouse is as yet unknown, however. Studies to determine this are presently underway.

Our analyses have determined some of the downstream transcript alterations that are the sequellae of mutations in *ldis1*. The principle transcripts that are downregulated in the RIIIS/J mouse include the γ-crystallins, a protein family responsible

for lens transparency. Demonstrative of their importance in lens physiology, several mutations in γ-crystallin genes have been associated with mouse models of cataract (reviewed in [1,3,26]). The pattern of expression of the transforming growth factor superfamily of proteins, including some TGFs, BMPs, and activins, is also dramatically altered in the RIIIS/J mouse. Members of this superfamily have been implicated in regulating lens maturation and differentiation [27] including terminal differentiation of lens fibers [28] as well as the initiation of differentiation [29]. Likewise, the GST transcript family is downregulated in eyes from RIIIS/J mutants compared to wildtype controls. The GSTs are ubiquitous enzymes that are critical for cellular detoxification due to their functions as antioxidants [30]. In the lens, oxidative stress is normally managed by the GSTs, thus cellular proteins, DNA, and organelles remain intact and cell death of the lens epithelium does not occur [31,32].

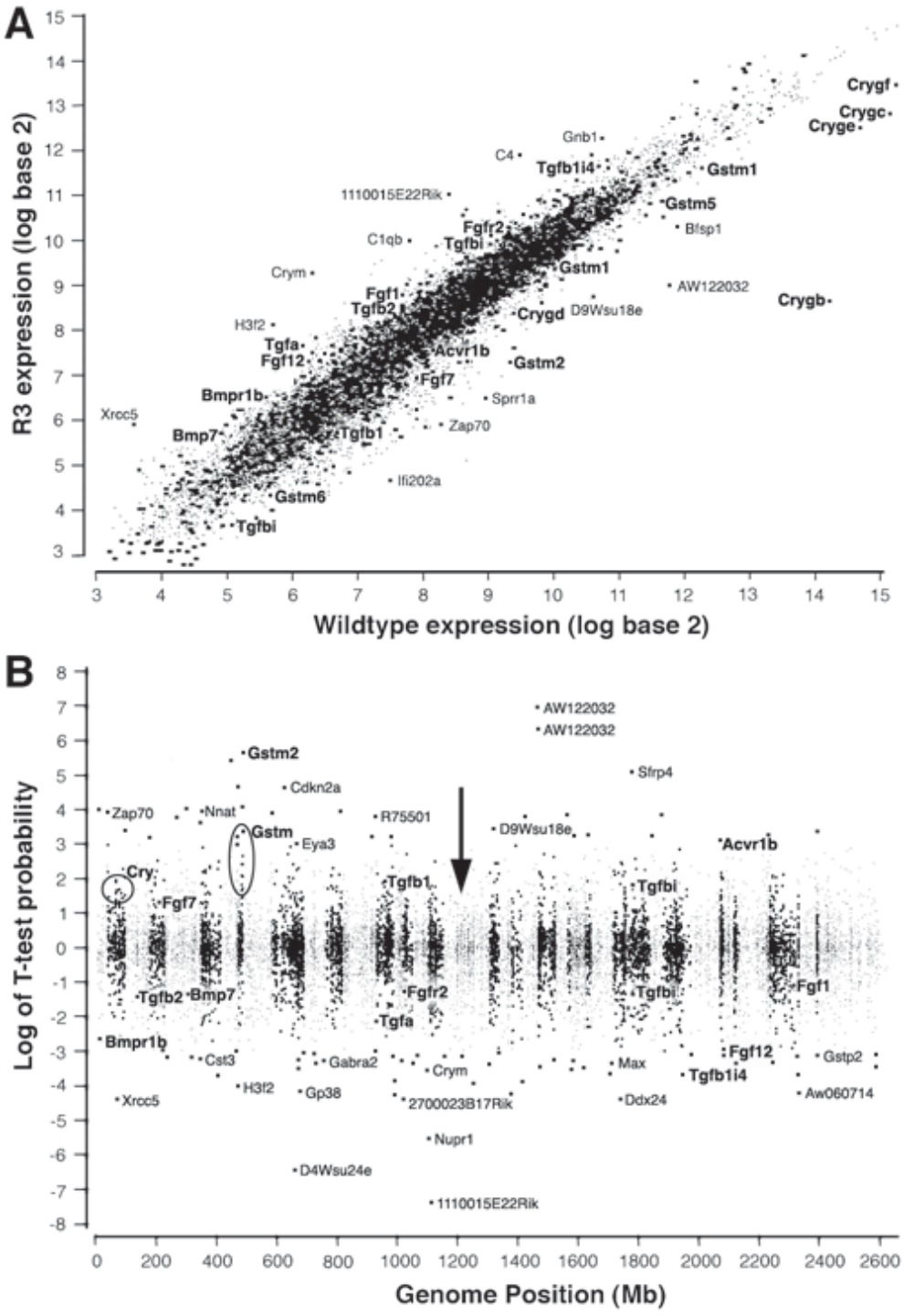

Figure 7. Comparative transcript mapping of whole eyes from RIIIS/J and wildtype mice. **A** contrasts the expression levels between the mutant and wildtype mice. **B** plots t-test scores (Y-axis) versus Genome location (X-axis; chromosome 1 to far left and chromosome Y to far right). Transcripts with a positive value indicate those that are expressed at a higher level in the wildtype controls while those with a negative value are higher in the RIIIS/J mutant mice. The arrow indicates location of the *ldis1* gene. In both panels, several γ-crystallins, TGF superfamily members, and GST transcripts that are significantly different in RIIIS/J eyes are highlighted in a bold and slightly larger font. Other transcripts are also noted.

Because multiple members of the γ-crystallins, the transforming growth factor, and glutatione S-transferase superfamilies are all reduced in eyes from the RIIIS/J mutant and their known role in lens and ocular health, it is highly probably that all three families contribute to the small eye and lens phenotype that we document in this mouse. While the genes of none of these family members lies in the 2-LOD support interval of *ldis1*, the expression levels of all of these are modified by a mutation in *ldis1*, demonstrating that although a mutation in a particular gene may not always alter its own level of expression, it may modify the levels of other downstream gene products that may ultimately lead to the aberrant phenotype and physiology of a tissue. These microarray studies were not intended to prove that the ocular phenotype of the RIIIS/J mutant mouse is due to alterations in the transcript level(s) of any particular gene product. Rather, they were undertaken to set the stage for subsequent analyses in which a time course of molecular alterations leading to the development of the phenotype could be determined in future studies.

ACKNOWLEDGEMENTS

The authors would like to thank Samuel Zigler for helpful discussions. They also thank Sharon Frase and the Integrated Microscopy Center at the University of Memphis for tissue processing and sectioning and William Orr at the University of Tennessee Health Science Center for assistance with the analysis of the microarray data. Supported in part by a Vision Core Grant (EY031080) and individual awards (EY13070 and EY12991 to RWW) from the National Eye Institute, and an unrestricted grant to the Department of Ophthalmology from Research to Prevent Blindness. MMJ is a recipient of the Research to Prevent Blindness William and Mary Greve Scholar Award.

REFERENCES

1. Hejtmancik JF, Smaoui N. Molecular genetics of cataract. Dev Ophthalmol 2003; 37:67-82.
2. Beebe DC, Coats JM. The lens organizes the anterior segment: specification of neural crest cell differentiation in the avian eye. Dev Biol 2000; 220:424-31.
3. Graw J, Loster J. Developmental genetics in ophthalmology. Ophthalmic Genet 2003; 24:1-33.
4. Hawes NL, Smith RS, Chang B, Davisson M, Heckenlively JR, John SW. Mouse fundus photography and angiography: a catalogue of normal and mutant phenotypes. Mol Vis 1999; 5:22 .
5. Semenova E, Wang X, Jablonski MM, Levorse J, Tilghman SM. An engineered 800 kilobase deletion of Uchl3 and Lmo7 on mouse chromosome 14 causes defects in viability, postnatal growth and degeneration of muscle and retina. Hum Mol Genet 2003; 12:1301-12.
6. Williams RW, Strom RC, Rice DS, Goldowitz D. Genetic and environmental control of variation in retinal ganglion cell number in mice. J Neurosci 1996; 16:7193-205.
7. Lu L, Airey DC, Williams RW. Complex trait analysis of the hippocampus: mapping and biometric analysis of two novel gene loci with specific effects on hippocampal structure in mice. J Neurosci 2001; 21:3503-14.
8. Don RH, Cox PT, Wainwright BJ, Baker K, Mattick JS. 'Touchdown' PCR to circumvent spurious priming during gene amplification. Nucleic Acids Res 1991; 19:4008.
9. Dietrich WF, Miller JC, Steen RG, Merchant M, Damron D, Nahf R, Gross A, Joyce DC, Wessel M, Dredge RD, Marquis A, Stein LD, Goodman N, Page DC, Lander ES. A genetic map of the mouse with 4,006 simple sequence length polymorphisms. Nat Genet 1994; 7:220-45.
10. Manly KF, Cudmore RH Jr, Meer JM. Map Manager QTX, cross-platform software for genetic mapping. Mamm Genome 2001; 12:930-2.
11. Haley CS, Knott SA. A simple regression method for mapping quantitative trait loci in line crosses using flanking markers. Heredity 1992; 69:315-324.
12. Churchill GA, Doerge RW. Empirical threshold values for quantitative trait mapping. Genetics 1994; 138:963-71.
13. Storey JD, Tibshirani R. Statistical significance for genomewide studies. Proc Natl Acad Sci U S A 2003; 100:9440-5.
14. Zhou G, Williams RW. Mouse models for the analysis of myopia: an analysis of variation in eye size of adult mice. Optom Vis Sci 1999; 76:408-18.
15. Zhou G, Williams RW. Eye1 and Eye2: gene loci that modulate eye size, lens weight, and retinal area in the mouse. Invest Ophthalmol Vis Sci 1999; 40:817-25.
16. Bu L, Jin Y, Shi Y, Chu R, Ban A, Eiberg H, Andres L, Jiang H, Zheng G, Qian M, Cui B, Xia Y, Liu J, Hu L, Zhao G, Hayden MR, Kong X. Mutant DNA-binding domain of HSF4 is associated with autosomal dominant lamellar and Marner cataract. Nat Genet 2002; 31:276-8.
17. Brady JP, Piatigorsky J. Cloning and characterization of a novel zinc-finger protein-encoding cDNA from the mouse eye lens. Gene 1993; 124:207-14.
18. Xu L, Overbeek PA, Reneker LW. Systematic analysis of E-, N- and P-cadherin expression in mouse eye development. Exp Eye Res 2002; 74:753-60.
19. Russ PK, Davidson MK, Hoffman LH, Haselton FR. Partial characterization of the human retinal endothelial cell tight and adherens junction complexes. Invest Ophthalmol Vis Sci 1998; 39:2479-85.
20. Heimark RL, Kaochar S, Stamer WD. Human Schlemm's canal cells express the endothelial adherens proteins, VE-cadherin and PECAM-1. Curr Eye Res 2002; 25:299-308.
21. Faulkner-Jones BE, Godinho LN, Tan SS. Multiple cadherin mRNA expression and developmental regulation of a novel cadherin in the developing mouse eye. Exp Neurol 1999; 156:316-25.
22. Honjo M, Tanihara H, Suzuki S, Tanaka T, Honda Y, Takeichi M. Differential expression of cadherin adhesion receptors in neural retina of the postnatal mouse. Invest Ophthalmol Vis Sci 2000; 41:546-51.
23. Saika S, Kawashima Y, Miyamoto T, Okada Y, Tanaka S, Yamanaka O, Ohnishi Y, Ooshima A, Yamanaka A. Immunolocalization of hyaluronan and CD44 in quiescent and proliferating human lens epithelial cells. J Cataract Refract Surg 1998; 24:1266-70.
24. Marner E. A family with eight generations of hereditary cataract. Acta Ophthal. 1949. 27: 537-551.
25. Eiberg H, Marner E, Rosenberg T, Mohr J. Marner's cataract (CAM) assigned to chromosome 16: linkage to haptoglobin. Clin Genet 1988; 34:272-5.
26. Hejtmancik JF. The genetics of cataract: our vision becomes clearer. Am J Hum Genet 1998; 62:520-5.
27. McAvoy JW, Chamberlain CG, de Iongh RU, Hales AM, Lovicu FJ. Lens development. Eye 1999; 13:425-37.
28. de Iongh RU, Lovicu FJ, Overbeek PA, Schneider MD, Joya J,

Hardeman ED, McAvoy JW. Requirement for TGFbeta receptor signaling during terminal lens fiber differentiation. Development 2001; 128:3995-4010.
29. Belecky-Adams TL, Adler R, Beebe DC. Bone morphogenetic protein signaling and the initiation of lens fiber cell differentiation. Development 2002; 129:3795-802.
30. Boyland E, Chasseaud LF. The role of glutathione and glutathione S-transferases in mercapturic acid biosynthesis. Adv Enzymol Relat Areas Mol Biol 1969; 32:173-219.
31. Fukagawa NK, Timblin CR, Buder-Hoffman S, Mossman BT. Strategies for evaluation of signaling pathways and transcription factors altered in aging. Antioxid Redox Signal 2000; 2:379-89.
32. Rosen P, Nawroth PP, King G, Moller W, Tritschler HJ, Packer L. The role of oxidative stress in the onset and progression of diabetes and its complications: a summary of a Congress Series sponsored by UNESCO-MCBN, the American Diabetes Association and the German Diabetes Society. Diabetes Metab Res Rev 2001; 17:189-212.

The print version of this article was created on 23 Aug 2004. This reflects all typographical corrections and errata to the article through that date. Details of any changes may be found in the online version of the article.